Understanding the effect of perturbations on the Gaussianity of various coordinates for the space object tracking problem

Shambo Bhattacharjee[a], John T. Kent[b], Weston R. Faber[c], Islam I. Hussein[d], and Moriba K. Jah[e]

[a]PhD Researcher, Department of Statistics, University of Leeds, Leeds, UK, mmsb@leeds.ac.uk
[b]Professor, Department of Statistics, University of Leeds, Leeds, UK, j.t.kent@leeds.ac.uk
[c]Aerospace Engineer, Applied Defense Solutions, Columbia, USA, wfaber@applieddefense.com
[d]Aerospace Engineer, Applied Defense Solutions, Columbia, USA, ihussein@applieddefense.com
[e]Professor, Department of Aerospace Engineering, University of Texas at Austin, Austin, USA, moriba@utexas.edu

ABSTRACT

Consider a space object in an orbit about the earth. An uncertain initial state can be represented as a point cloud which can be propagated to later times by the laws of Newtonian motion. However, even if the initial uncertainty is Gaussian in ECI coordinates, the distribution quickly becomes non-Gaussian as the propagation time increases. Similar problems arise in other standard fixed coordinate systems in astrodynamics, e.g. Keplerian and to some extent equinoctial. To address this problem, a local "Adapted Structural (AST)" coordinate system has been developed in which uncertainty is represented in terms of deviations from a "central state". In AST coordinates, the propagated uncertainty is nearly Gaussian under a wide range of conditions (e.g. LEO vs. GEO; varying eccentricity, varying initial uncertainty). Most of the assessment has been carried out so far in Keplerian dynamics. In this paper, we explore the behavior of AST coordinates when perturbation effects are incorporated, namely atmospheric drag and oblateness. The behavior of AST is assessed visually through pairs plots and statistically through tests of Gaussianity

Keywords: Uncertainty Propagation, point cloud, Adapted STructural (AST) coordinate system, Perturbation effects, Normality analysis

1. INTRODUCTION

Uncertainty propagation is a fundamental issue in orbital mechanics for the purpose of object tracking and association problems. For example, J.L. Junkins, M. Akella, and K. Alfriend [2] studied nonlinear characteristics of the propagated uncertainty under different coordinate systems. They used a Monte Carlo simulation based approach. I. Park and D.J. Scheeres [8] used a mixture (hybrid approach) of a simplified dynamic system (SDS) model and the state transition tensor (STT) model to propagate and model the uncertainty. V. Vittaldev, R.P. Russell and R. Linares [9] proposed a mixture of polynomial chaos expansion and Gaussian Mixture Models (GMM). J.T. Horwood and A.B. Poore [4] proposed a Gauss Von Mises (GVM) filter. Further, the paper by G.R. Hintz [10] provides a concise summary on different coordinate systems. However, most of the mentioned papers used *fixed* coordinate systems to perform uncertainty analysis.

The approach promoted in this paper uses instead a *local* or *adapted* coordinate system. Imagine the distribution of a noisy state is represented in terms of a "central" state surrounded by a point cloud of nearby states. Then choose a coordinate system centered at the central state in such a way that the uncertainty is approximately Gaussian distributed.

Consider a space object in orbit about the earth. If the initial location and velocity, $\boldsymbol{x}(0)$ and $\dot{\boldsymbol{x}}(0)$, are known 3-dimensional vectors at time $t = 0$, then the laws of Newtonian motion can be used to propagate the motion to $\boldsymbol{x}(t)$ and $\dot{\boldsymbol{x}}(t)$ for all $t > 0$. Similarly, given a probability distribution to describe a noisy initial position and velocity (such as 6-dimensional Gaussian), it is possible to simulate a random initial position $\boldsymbol{x}^{\text{rand}}(0)$ and velocity $\dot{\boldsymbol{x}}^{\text{rand}}(0)$, and to propagate these to give $\boldsymbol{x}^{\text{rand}}(t)$ and $\dot{\boldsymbol{x}}^{\text{rand}}(t)$ for $t > 0$. Given a simulated point cloud

of N initial conditions, $\boldsymbol{x}_j(0)$ and $\dot{\boldsymbol{x}}_j(0)$, $j = 1, \ldots, N$, where N is typically large, it is possible to follow the evolution of the point cloud in time.

It is well-known that as t increases, the shape of the point cloud for position $\boldsymbol{x}(t)$ becomes more "banana-shaped" in $\mathbb{R}^3$.[1,2] This distribution is awkward to describe analytically. In order to address this problem, we previously introduced an "Adapted STructural (AST)" coordinate system.[5,15] It is a "structural" coordinate system because, just as Keplerian elements do, it represents the underlying structural parameters of the orbit (such as ellipticity and normal direction of the orbital plane). In addition it is "local" because the AST coordinates represent deviations about a "central" state.

AST coordinates are available in a number of mild variants, and this paper proposes a new variant.

The key contributions of this paper are as follows.

(a) We review the problems of non-Gaussianity in the propagation of point clouds under different standard coordinate systems.

(b) We introduce a new variant of AST coordinates and show explicitly how they can be represented in terms of deviations in ECI coordinates using a first order Taylor series expansion.

(c) Next, we illustrate how perturbation effects, such as oblateness and atmospheric drag, affect the distribution of propagated AST coordinates.

(d) Finally, we use statistical tests of Gaussianity to assess the approximate Gaussianity of the propagated AST coordinates under perturbed dynamics.

2. STANDARD ASTRODYNAMIC COORDINATE SYSTEMS

The standard coordinate systems to represent the state of an orbiting object include the following:

- **Cartesian ECI coordinates:** A state is represented by a three-dimensional position vector and a three-dimensional velocity vector.
- **Keplerian orbital elements:** A state is the represented using semi-major axis (a), eccentricity (e), inclination (i), RAAN (Ω), argument of perigee (ω) and wrapped mean anomaly (M_0).
- **Equinoctial orbital elements:** A state is represented using a, $h = e\sin(\Omega+\omega)$, $k = e\cos(\Omega+\omega)$, $p = \tan(i/2)\sin(\Omega)$, $q = \tan(i/2)\cos(\Omega)$ and $\lambda = \Omega + \omega + M_0$.

Hintz [10] provides an extensive list of other coordinate systems, such as modified equinoctial elements, Euler parameter sets, Delaunay elements, Poincaré elements etc., but they are all fixed coordinate systems and they have similar problems to the ones examined here. For this section we use Keplerian dynamics to propagate the point clouds, since the problems of non-Gaussianity arise even in this idealized situation.

Example 1. Consider an orbiting LEO object in a prograde equatorial orbit, with eccentricity 0.01 and orbital period 99.5 minutes, and whose initial state in Cartesian ECI coordinates is uncertain, with standard deviation = 1 km for each location coordinate and 0.005 km/sec for each velocity coordinate, where the uncertainties in all 6 coordinates are independent. These initial uncertainties are realistic and moderate.

The state of the object has been propagated for 2.09 days (approximately 30.25 orbits for the central state). Propagated point clouds have represented as 6-dimensional pairs plot in Cartesian ECI (Fig. 1), Keplerian (Fig. 2) and Equinoctial (Fig. 3) coordinates. For all the examples we use $N = 2000$ data points to generate the point cloud. This value suffices to visualise key features in the pairs plots such as skewness, outliers, and approximate Gaussianity.

Many of the bivariate scatterplots exhibit extreme non-Gaussianity. Here are some instances.

(a) In **ECI coordinates** (Fig. 1), most of the scatter plots, related to coordinates 2 and 4 are showing curvature.

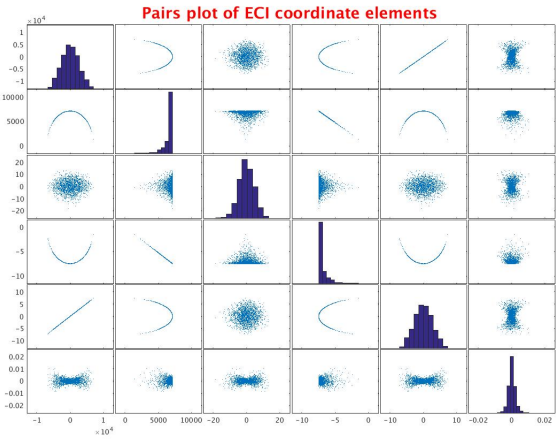

Figure 1. **Example 1.** Propagated point cloud in Cartesian ECI coordinates for the three position and three velocity coordinates.

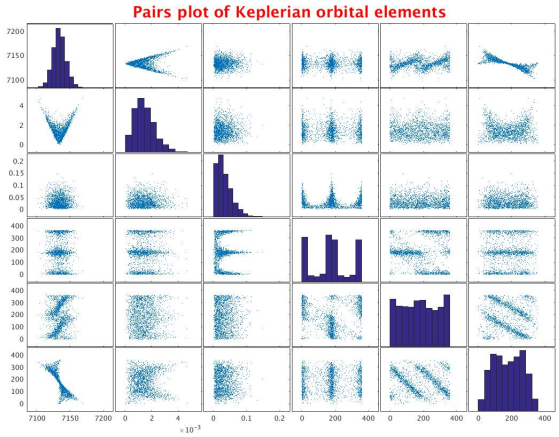

Figure 2. **Example 1.** Propagated point cloud in Keplerian coordinates.

(b) In **Keplerian coordinates** (Fig. 2), the scatter plot for coordinates 1 in 2 has a "V" shape, due partly to the fact that the eccentricity has a lower bound of 0. The range for the angular coordinates 4 and 5 (RAAN and argument of perigee) covers the whole circle because the central orbit is equatorial; these variables also have bimodal distributions.

(c) In **Equinoctial coordinates** (Fig. 3) all the scatterplots look approximately Gaussian for this example.

Example 2. In the same setting as Example 1, increase the initial standard deviations to 30 km and 0.6 km/sec respectively. The pairs plot in equinoctial coordinates is given in Fig. 4 (propagation time = 30.25 orbits compared to the central state). Then a scatter plot for variables 1 and 2 shows some curvature. Equinoctial coordinates also have problems for retrograde orbits.

3. THE ADAPTED STRUCTURAL (AST) COORDINATE SYSTEM

The AST coordinate system is made of 6 coordinates.

(a) one coordinate, the change in true anomaly between a state in the point cloud from the central state at $t = 0$.

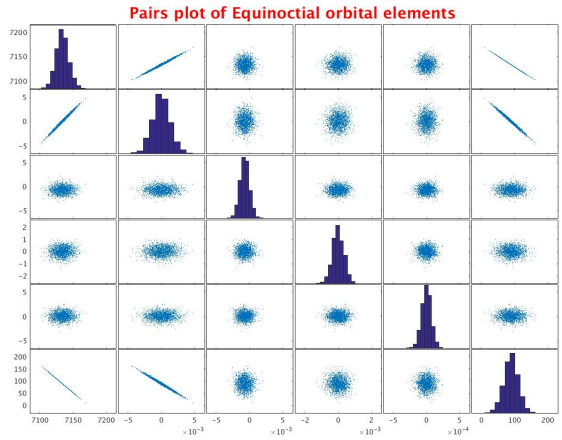

Figure 3. **Example 1.** Propagated point cloud in equinoctial coordinates

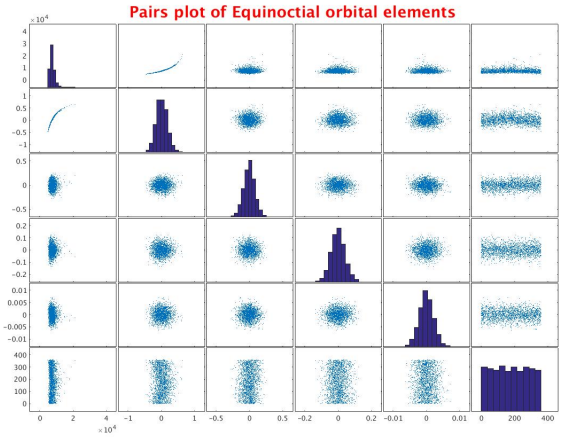

Figure 4. **Example 2, with increased uncertainty.** Propagated point cloud in equinoctial coordinates

(b) two coordinates to describe the normal direction to the elliptical plane,

(c) two coordinates to describe the direction of the major axis and eccentricity, and

(d) one coordinate, the mean motion, to describe the location of the object along the ellipse.

3.1 Construction of the AST coordinate system

Before describing the construction of AST coordinates, it is helpful to recall some standard results from the orbital mechanics.[7] The cross product

$$\boldsymbol{h} = \boldsymbol{x}(t) \times \dot{\boldsymbol{x}}(t).$$

is called the specific angular momentum vector. Express $\boldsymbol{h} = h\boldsymbol{n}$ where h is the magnitude of $\boldsymbol{h}$ and $\boldsymbol{n} = \boldsymbol{h}/|\boldsymbol{h}|$ is the unit vector proportional to $\boldsymbol{h}$. Other standard notation includes $r(t)$ for the altitude at time t, $\boldsymbol{e}$ for the eccentricity vector, e for the eccentricity, r_p and r_a for the radius from perigee and apogee respectively, a for the semi-major axis, b for the semi-minor axis, ξ for the mean motion, and finally T for the orbital time period

. These quantities are given by

$$
\begin{aligned}
&r(t) = \sqrt{\boldsymbol{x}(t) \cdot \boldsymbol{x}(t)}, \quad \boldsymbol{e} = \frac{1}{\mu}(\dot{\boldsymbol{x}}(t) \times \boldsymbol{h} - \mu \frac{\boldsymbol{x}(t)}{r}), \\
&e = \sqrt{\boldsymbol{e} \cdot \boldsymbol{e}}, \quad r_p = \frac{h^2}{\mu} \frac{1}{1+e}, \quad r_a = \frac{h^2}{\mu} \frac{1}{1-e}, \\
&a = \frac{1}{2}(r_p + r_a), \quad b = \frac{a}{\sqrt{1-e^2}}, \\
&\xi = \sqrt{\frac{\mu}{a^3}} T = \frac{2\pi}{\sqrt{\mu}} a^{\frac{3}{2}},
\end{aligned}
$$

where μ is the standard gravitational constant. Under Keplerian dynamics, apart from $r(t)$, all these parameters are time invariant.

Next we describe the construction of AST coordinates. This task requires care because the purpose of AST coordinates is to describe the uncertainty in the state of an orbiting object. Suppose that a *central state* $(\boldsymbol{x}_c(0), \dot{\boldsymbol{x}}_c(0))$ sitting near the middle of the point cloud at time $t = 0$ has been highlighted. The central state will be used as a "base" for our coordinate system about which certain "tangent coordinates" will be constructed.

(a) Let $R = [\boldsymbol{u}, \boldsymbol{v}, , \boldsymbol{w}]$ be a 3×3 rotation matrix defined in terms of the central state, where the three columns are orthogonal unit vectors defined by

$$
\begin{aligned}
&\boldsymbol{u} \propto \boldsymbol{x}_c(0), \\
&\boldsymbol{v} \propto \dot{\boldsymbol{x}}_c(0) - \dot{\boldsymbol{x}}_c(0)^T \boldsymbol{u}, \\
&\boldsymbol{w} = \boldsymbol{n} \propto \boldsymbol{h}.
\end{aligned}
$$

Let $\boldsymbol{y}_c(t) = R^T \boldsymbol{x}_c(t)$, $\dot{\boldsymbol{y}}_c(t) = R^T \dot{\boldsymbol{x}}_c(t)$ and $\boldsymbol{y}^{\text{rand}}(t) = R^T \boldsymbol{x}^{\text{rand}}(t)$, $\dot{\boldsymbol{y}}^{\text{rand}}(t) = R^T \dot{\boldsymbol{x}}^{\text{rand}}(t)$ denote the rotated versions of the central state and states in the point cloud. Then the central state at time $t = 0$ must take the form

$$
\boldsymbol{y}(0) = \begin{bmatrix} A \\ 0 \\ 0 \end{bmatrix}, \quad \dot{\boldsymbol{y}}(0) = \begin{bmatrix} B \\ C \\ 0 \end{bmatrix}, \tag{1}
$$

where A, B, C are real numbers with $A = r(0) > 0$ and $C > 0$.

(b) For simplicity we work in the y frame of reference for the rest of this section. We assume small deviations between the initial point cloud and the initial central state. Hence, the normal direction for a state in the point cloud $\boldsymbol{n}^{\text{rand}}(0)$ will be close to the normal direction for the central state, that is, the vertical direction $\boldsymbol{n}_c(0) = [0, 0, 1]^T$. In particular the first two coordinates $\boldsymbol{n}_1^{\text{rand}}(0)$, $\boldsymbol{n}_2^{\text{rand}}(0)$ describe the departure from vertical.

(c) The ellipticity vector $\boldsymbol{e}^{\text{rand}}(0)$ for a state in the point cloud will nearly lie in the horizontal plane. The interesting information is in the first two components; the third component $\boldsymbol{e}_3^{\text{rand}}(0)$ will be nearly zero.

(d) Two further pieces of information needed to specify a random state at time t are the size of the orbital ellipse and the position of the orbiting object along the ellipse. These are determined by the quantity h^{rand} and the mean anomaly

$$
M(t) = \xi^{\text{rand}} t \tag{2}
$$

where

$$
\xi^{\text{rand}} = \sqrt{\mu / (a^{\text{rand}})^3}
$$

is the mean motion.

(e) The change in true anomaly between a state in the point cloud from the central state at $t = 0$ can be computed as,

$$\psi^{\text{rand}} = \text{atan2}(\boldsymbol{y}^{\text{rand}}{}_2(0), \boldsymbol{y}^{\text{rand}}{}_1(0)) - \text{atan2}(\boldsymbol{y}_2(0), \boldsymbol{y}_1(0)) \tag{3}$$

(f) Putting the pieces together, we define the AST coordinates for a random element of the point cloud to be

$$\psi^{\text{rand}},\ n_1^{\text{rand}}, n_2^{\text{rand}},\ e_1^{\text{rand}}, e_2^{\text{rand}},\ \xi^{\text{rand}}.$$

Note that under Keplerian dynamics none of these coordinates varies with t. The effect of t on the location of the object along its orbit is governed by (2).

3.2 Propagation in AST coordinates

Example 1, continued. First, we show the propagation in AST coordinates using same initial conditions (plus uncertainties mentioned in Example 1), in Fig. 5 all the AST coordinates can be approximated using univariate normal distribution.

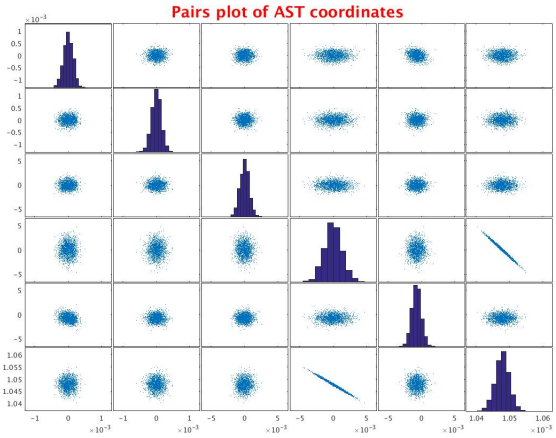

Figure 5. **Example 1, continued.** Propagated point cloud ($N = 2000$) in AST coordinates

Example 2, continued. Example 2 is a good test of a coordinate system because the initial uncertainties are large. A pairs plot for AST coordinates is given in Fig. 6. All the one-dimensional histograms and all the two-dimensional scatter plots appear to be approximately Gaussian.

3.3 A first order representation for AST coordinates

In the y frame of reference, assume that a random state at time $t = 0$ is a small deviation from the central state in (1); that is,

$$\boldsymbol{y}^{\text{rand}}(0) = \begin{bmatrix} A + \epsilon_1 \\ \epsilon_2 \\ \epsilon_3 \end{bmatrix}, \quad \dot{\boldsymbol{y}}^{\text{rand}}(0) = \begin{bmatrix} B + \delta_1 \\ C + \delta_2 \\ \delta_3 \end{bmatrix}$$

where $\boldsymbol{\epsilon}$ and $\boldsymbol{\delta}$ are "small". In this section we derive first order expressions for the AST coordinates in terms of $\boldsymbol{\epsilon}$ and $\boldsymbol{\delta}$. In all the expansions second and higher order effects are ignored. The calculations are split into groups.

The change in true anomaly. The change in true anomaly between a state in the point cloud from the central state at $t = 0$, can be computed using 3

$$\psi^{\text{rand}} = \text{atan2}(\epsilon_2, A + \epsilon_1) - \text{atan2}(0, A) \approx \epsilon_2/A - 0 = \epsilon_2/A.$$

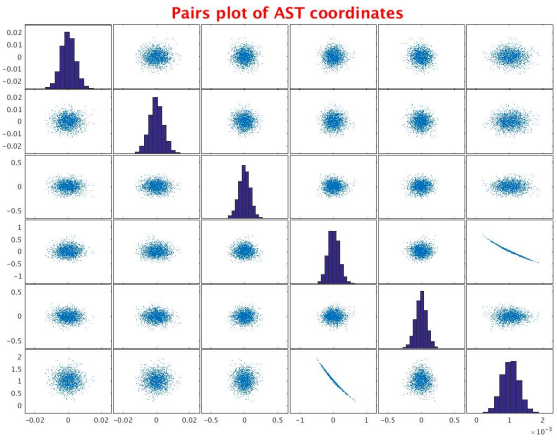

Figure 6. **Example 2, continued.** Propagated point cloud ($N = 2000$) in AST coordinates

The angular momentum vector. This vector can be expressed as

$$\begin{aligned}\boldsymbol{h}^{\text{rand}} &= \boldsymbol{y}^{\text{rand}} \times \dot{\boldsymbol{y}}^{\text{rand}} \\ &= \begin{bmatrix} \epsilon_2\delta_3 - \epsilon_3(C+\delta_2) \\ \epsilon_3(B+\delta_1) - (A+\epsilon_1)\delta_3 \\ (A+\epsilon_1)(C+\delta_2) - \epsilon_2(B+\delta_1) \end{bmatrix} \\ &\approx \begin{bmatrix} -\epsilon_3 C \\ \epsilon_3 B - A\delta_3 \\ AC + A\delta_2 + C\epsilon_1 - \epsilon_2 B \end{bmatrix}\end{aligned}$$

with squared norm

$$(h^{\text{rand}})^2 \approx A^2C^2 + 2AC(A\delta_2 + C\epsilon_1 - B\epsilon_2).$$

Further, the first two components of $\boldsymbol{n}^{\text{rand}} = \boldsymbol{h}^{\text{rand}}/h^{\text{rand}}$ simplify to

$$n_1^{\text{rand}} = -\epsilon_3 C, \qquad n_2^{\text{rand}} = \epsilon_3 B - A\delta_3$$

The eccentricity vector. After a bit of calculation, the expression for the eccentricity vector $\boldsymbol{e}^{\text{rand}}$ simplifies to

$$\boldsymbol{e}^{\text{rand}} = \frac{1}{\mu}\begin{bmatrix} AC^2 + 2\delta_2 AC + \epsilon_1 C^2 - \epsilon_2 BC - \mu - \mu\epsilon_1/A \\ -ABC - \delta_1 AC - \epsilon_1 BC - \delta_2 AB + \epsilon_2 B^2 - \mu\epsilon_2/A \\ -\delta_3 AB - \epsilon_3 B^2 - \epsilon_3 C^2 - \mu\epsilon_3/A \end{bmatrix}.$$

Hence

$$\begin{aligned} e_1^{\text{rand}} &= \frac{1}{\mu}(AC^2 + 2\delta_2 AC + \epsilon_1 C^2 - \epsilon_2 BC - \mu - \mu\epsilon_1/A), \\ e_2^{\text{rand}} &= \frac{1}{\mu}(-ABC - \delta_1 AC - \epsilon_1 BC - \delta_2 AB + \epsilon_2 B^2 - \mu\epsilon_2/A). \end{aligned}$$

The mean motion. From $\boldsymbol{e}^{\text{rand}}$, we can compute its squared norm

$$\begin{aligned} e^{\text{rand}\,2} =& \frac{1}{\mu^2}\{(AC^2 - \mu)^2 \\ &+ 2(2\delta_2 AC + \epsilon_1 C^2 - \epsilon_2 BC - \mu\epsilon_1/A)(AC^2 - \mu) \\ &+ (ABC)^2 \\ &+ 2(\delta_1 AC + \epsilon_1 BC + \delta_2 AB - \epsilon_2 B^2 + \mu\epsilon_2/A)(ABC)\}. \end{aligned}$$

Write

$$(e^{\text{rand}})^2 = {e_c}^2 + f_e^{\text{rand}},$$

where ${e_c}^2$ denotes the eccentricity for the central state and write

$$(h^{\text{rand}})^2 = h_c^2 + f_h^{\text{rand}},$$

where h_c denotes the magnitude of the central angular momentum vector. Then

$$\begin{aligned} e_c^2 &= \frac{1}{\mu^2}\{(AC^2-\mu)^2 + (ABC)^2\}, \\ f_e^{\text{rand}} \approx &\frac{1}{\mu^2}\{2(2\delta_2 AC + \epsilon_1 C^2 - \epsilon_2 BC - \mu\epsilon_1/A)(AC^2-\mu) \\ &+ 2(\delta_1 AC + \epsilon_1 BC + \delta_2 AB - \epsilon_2 B^2 + \mu\epsilon_2/A)(ABC)\}, \\ h_c^2 &= A^2C^2, \\ f_h^{\text{rand}} &= 2AC(A\delta_2 + C\epsilon_1 - B\epsilon_2). \end{aligned}$$

Then a^{rand} takes the form

$$\begin{aligned} a^{\text{rand}} &= \frac{(h^{\text{rand}})^2}{\mu}\frac{1}{1-(e^{\text{rand}})^2} \\ &\approx \frac{{h_c}^2}{\mu}\frac{1}{1-e_c^2}(1 + \frac{f_h^{\text{rand}}}{h_c^2} + \frac{f_e^{\text{rand}}}{1-(e^{\text{rand}})^2}) \\ &= a_c + f_a^{\text{rand}}, \end{aligned}$$

where

$$a_c = \frac{h_c^2}{\mu}\frac{1}{1-e_c^2} \text{ and } f_a^{\text{rand}} = a_c(\frac{f_h^{\text{rand}}}{h_c^2} + \frac{f_e^{\text{rand}}}{1-(e^{\text{rand}})^2}).$$

Finally, if we write $\xi^{\text{rand}} = \sqrt{\mu/(a^{\text{rand}})^3}$ in the form $\xi^{\text{rand}} = \xi_c + f_\xi^{\text{rand}}$, then

$$\begin{aligned} \xi^{\text{rand}} &= \sqrt{\frac{\mu}{(a_c + f_a^{\text{rand}})^3}} \\ &\approx \sqrt{\frac{\mu}{{a_c}^3}}(1 - \frac{3}{2}\frac{f_{a*}}{a_c}) \\ &\approx \xi_c(1 - \frac{3}{2}\frac{f_a^{\text{rand}}}{a_c}) \\ &\approx \xi_c - \frac{3}{2}\frac{f_a^{\text{rand}}}{a_c}\xi_c \\ &\approx \xi_c + f_\xi^{\text{rand}}, \text{ say.} \end{aligned}$$

By putting these final expressions together, we can express the deviation f_ξ^{rand} in terms of $\boldsymbol{\epsilon}$ and $\boldsymbol{\delta}$.

3.4 Linearity analysis for AST state vectors

Next, we perform a linearity analysis for the AST coordinates to see to what extent the AST coordinates depend linearly on $\boldsymbol{\epsilon}$ and $\boldsymbol{\delta}$. For each component of $\boldsymbol{\epsilon}$ and $\boldsymbol{\delta}$, 20 equally spaced values were chosen in the interval ± 2 standard deviations, using the uncertainties from Example 1. Then with the other 5 components held fixed, the effect on the AST coordinates is shown as a pairs plot. A different color is used for each component (black, red and green for the three components of $\boldsymbol{\epsilon}$ and blue, cyan, violet for the three components of $\boldsymbol{\delta}$). The plots are all superimposed in Fig. 7.

We can see that velocity uncertainties are having maximum impact of AST coordinates and only one position uncertainty (Z or ϵ_3) have significant impact AST coordinates.

In Fig. 7 , scatters plots are extremely helpful for judging dependency among AST coordinates. From the scatter plots 1 *vs.* 2, 1 *vs.* 3, 1 *vs.* 4, 1 *vs.* 5, 1 *vs.* 6 we can say that the change in Y axis (${h_1}^{\text{rand}}, {h_2}^{\text{rand}}, {e_1}^{\text{rand}}, {e_2}^{\text{rand}}, \xi^{\text{rand}}$) is 0 with respect to the X-axis or ψ^{rand} and we can almost see a straight line. On the other hand, ${e_1}^{\text{rand}}$ and ξ^{rand} are highly correlated (correlation close to 1).

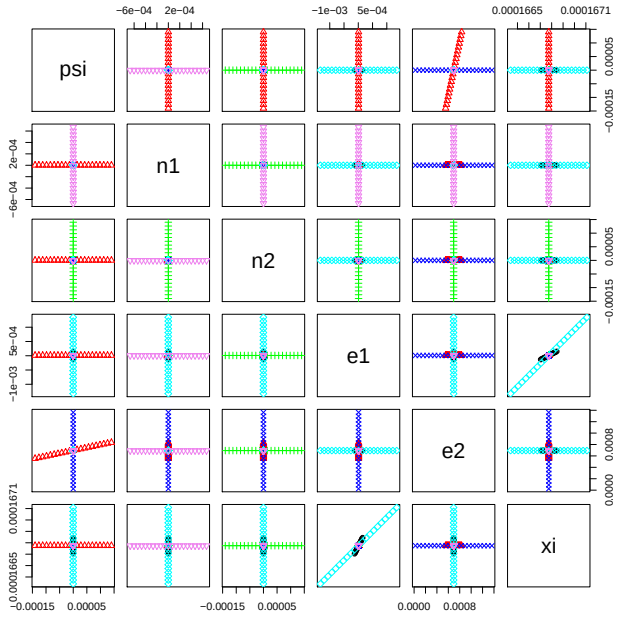

Figure 7. **Example 1.** Linearity analysis for AST state vectors

4. INCORPORATING NON-KEPLERIAN PERTURBATION EFFECTS

The preceding sections all used Keplerian dynamics. In this section we incorporate two different perturbation effects: oblateness and atmospheric drag. Since atmospheric drag is dominant in LEO orbit orbit we emphasize this situation. For modelling oblateness (J_2 effect), we have followed the model proposed by J.H. Jo et al.[17]

To visualize the impact of the atmospheric drag, we consider the standard drag model. Acceleration due to

atmospheric drag are computed using Gauss equation of motion, which are given below [17][18] -

$$
\begin{aligned}
da &= 2\frac{a^2}{\sqrt{\mu p}}[f_r e \sin\theta + f_\theta \frac{p}{r}], \\
de &= \frac{1}{\sqrt{\mu p}}[f_r p \sin\theta + f_\theta((p+r)\cos\theta + re], \\
di &= f_h \frac{r}{\sqrt{\mu p}} \cos(\Omega+\omega), \\
d\Omega &= f_h \frac{r}{\sqrt{\mu p}\sin i} \sin(\Omega+\omega), \\
d\omega &= -\sqrt{\frac{p}{\mu}}[f_h \frac{r}{p} \cot i \sin(\Omega+\omega) + \\
&\quad \frac{1}{e}(f_r \cos\theta - f_\theta(1+\frac{r}{p}) \sin\theta], \\
dM &= n - f_r[\frac{2r}{\sqrt{\mu}a} - \frac{1-e^2}{e}\sqrt{\frac{a}{\mu}} \cos\theta] - \\
&\quad f_\theta \frac{1-e^2}{e}\sqrt{\frac{a}{\mu}}(1+\frac{r}{p}) \sin\theta
\end{aligned}
$$

Further,

$$
r = a\frac{1-e^2}{1+e\cos\theta}
$$

Here, $\theta, a, r, \mu, E, \omega, i, e, n$ (or ξ in our notation) denote true anomaly, semi major axis length, radial distance, gravitational constant, eccentric anomaly, argument of perigee, inclination angle, mean motion respectively. Further, $da, de, di, d\Omega, d\omega, dM$ indicate small changes in major axis length, eccentricity, inclination angle, RAAN, argument of perigee and mean anomaly respectively. In this paper, we have iteratively added both perturbations after every single orbit.

Example 3. Here we have considered the same initial conditions that we used in example 1. In this section we describe impact of perturbations on AST coordinates. We considered two types of propagations: a) short term (30.25 orbital periods compared to the central orbit) and, b) long term (100.25 orbital periods compared to the central state). The results are summarized using Figs. 8 and 9.

Note that, under Keplerian dynamics, if we propagate the point cloud then only the last element (ξ or ξt) changes with time, other elements remain fixed. However, under non-Keplerian dynamics (after incorporating perturbation effects), all the elements show significant amount of change in their means and variances.

Fig. 8 and 9 indicate perturbed AST coordinates after $t = 30.25$ and 100.25 orbits. These plots (Figs. 8 and 9) are useful for visualizing normality. However, they don't provide enough information regarding change of variances. In Table 1, we compare variances between Fig. 8 and Fig. 9 and it shows that, if we propagate for a long time then variances change significantly for AST coordinates.

Table 1. Comparing variances between Fig. 8 and Fig. 9

AST coordinate	variance (Fig. 8)	variance (Fig. 9)	change (%)
Change in true anomaly	0.761131E-04	1.63448E-04	114.74
Angular momentum vector 1	0.000194E-04	0.000202E-04	4.32
Angular momentum vector 2	0.022133E-04	0.029858E-04	34.90
Eccentricity vector 1	0.081489E-04	0.118658E-04	45.61
Eccentricity vector 2	0.022553E-04	0.029786E-04	32.07
mean motion	0.02E-09	0.029E-09	44.85

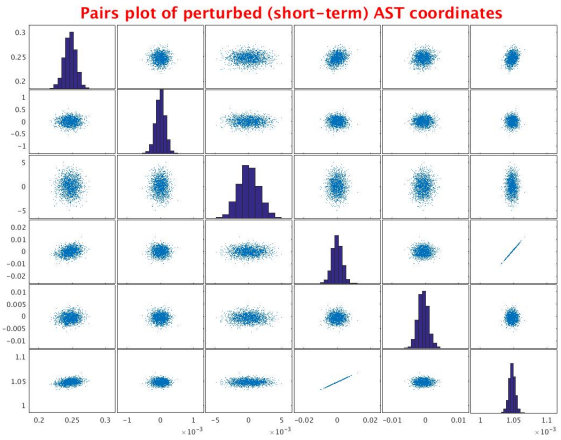

Figure 8. **Example-2:** Propagated point cloud ($N = 2000$) in AST coordinates, using non-Keplerian dynamics and short-term propagation.

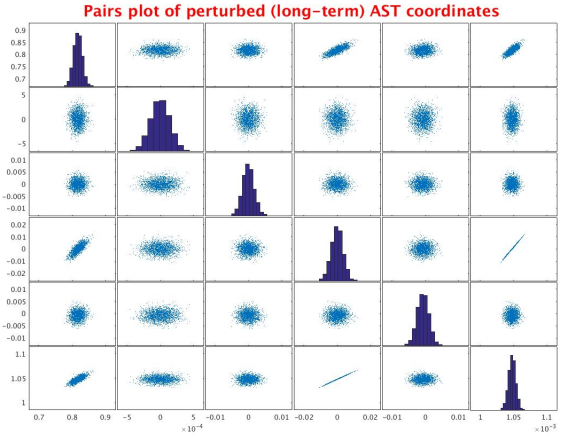

Figure 9. **Example-2:** Propagated point cloud ($N = 2000$) in AST coordinates, using non-Keplerian dynamics and long-term propagation.

5. STATISTICAL ANALYSIS

So far, we have judged normality in histograms or scatterplots by visual assessment. However, it is possible to take a more formal approach to these assessments using statistical tests. Two suitable test statistics were developed by Mardia [13] to assess skewness and kurtosis, respectively. These tests can be used on point clouds in all dimensions and have been implemented in the R programming language .[20] For our purposes we shall apply the tests to pairs of variables (e.g. as shown visually in the scatterplots). The results of each test can be summarized by a p-value. If normality holds, the p-value will be uniformly distributed between 0 and 1. However, if normality fails, then the p-value will tend to be close to 0. To carry out the statistical test, a small threshold α is chosen (e.g. $\alpha = 0.05$) and if the p-value is below the threshold, then the hypothesis of normality is rejected. For each figure, two p-values have been computed, one for skewness , and another for kurtosis.

The p-values for the examples in this paper are summarized in Table 2. Several features are of interest. For Cartesian-ECI coordinates, many of the propagated variables and pairs of variables dramatically fail the normality test. These results reinforce our visual impression. On the other hand, for AST coordinates (Figs. 5, 6, 8 and 9) p-values are greater than 0.05.

Caution- The power of a statistical test depends on the sample size (here the number of simulated points in the point cloud). If the underlying distribution is even slightly non-normal, then for a large enough sample size, the hypothesis of normality will be eventually rejected. Here we have used a sample size of $N = 2000$, which is adequate to confirm the approximate normality in Figs. 3, 5, 6, 8, 9 and to strongly reject normality in most of the plots in Figs. 1, 2 and 4.

Table 2. Normality test results, here $\boldsymbol{P_{skewness}}, \boldsymbol{P_{kurtosis}}$ p values for skewness and kurtosis respectively.

Figure details.	$\boldsymbol{P_{skewness}}$	$\boldsymbol{P_{kurtosis}}$
Cartesian-ECI	0	0
Keplerian	0	0
Equinoctial	**0.5**	**0.61**
Equinoctial (increased uncertainty)	0	0
AST coordinates	**0.3**	**0.23**
AST coordinates (increased uncertainty)	**0.55**	**0.7**
Perturbed AST (short-term)	**0.3**	**0.27**
Perturbed AST (long-term)	**0.11**	**0.1**

6. CONCLUSION

To summarize, in this paper we motivated the reason for constructing AST coordinates, and gave a new variant which has a more intuitive construction and interpretation. Further we gave a first order expansion in terms of deviations from a central state. This expansion demonstrated that AST coordinates are approximately linear functions of the deviations from a central state and helps explain why AST coordinates are generally typically approximately Gaussian whatever the initial conditions are.

Finally, we incorporated two perturbation effects from Keplerian dynamics and showed empirically that for large and moderate propagation times, the AST coordinates are still approximately Gaussian, though with a larger covariance matrix than under Keplerian dynamics.

Acknowledgment

This material is based upon work supported by the Air Force Office of Scientific Research, Air Force Materiel Command, USAF under Award No. FA9550-16-1-0099.

REFERENCES

[1] J. T. Kent, S. Bhattacharjee, I. I. Hussein, M. K. Jah, "Geometric restructurization of the space object tracking problem for improved uncertainty representation," 7th European Conference on Space Debris, Darmstadt, Germany, 2017.

[2] J.L.Junkins, M.R. Akella, K.T. Alfriend, "Non-Gaussian error propagation in orbital mechanics," Journal of the Astronautical Sciences, vol. 44, pp. 541–563, 1996.

[3] M Valli, R Armellin, P.D. Lizia, M.R Lavgna, "Non linear mapping of uncertainties in celestial mechanics," Journal of Guidance,Control and Dynamics, vol. 36, pp. 48–63, 2013.

[4] J. T. Horwood, A. B. Poore, "Non linear mapping of uncertainties in celestial mechanics, Gauss von Mises Distribution for Improved Uncertainty Realism in Space Situational Awareness," SIAM/ASA J. Uncertainty Quantification, vol. 2, pp. 276-304, 2014.

[5] J. T. Kent, S. Bhattacharjee, I. I. Hussein, M. K. Jah,"Nonlinear filtering using directional statistics for the orbital tracking problem with perturbation effects," Proceedings of the 28th AAS/AIAA Space Flight Mechanics Meeting, 2018.

[6] S. J. Julier and J. K. Uhlmann, "Unscented Filtering and Nonlinear Estimation," IEEE Proc., vol. 92, pp. 401–422, 2004.

[7] H. Curtis, "Orbital Mechanics for Engineering Students," Elsevier Aerospace Engineering Series, pp. 149–187, 2006.

[8] Inkwan Park and Daniel J. Scheeres. Hybrid Method for Uncertainty Propagation of Orbital Motion, Journal of Guidance, Control, and Dynamics, Vol. 41, No. 1, pp. 240–254, 2018.

[9] Vivek Vittaldev, Ryan P. Russell, and Richard Linares, Spacecraft Uncertainty Propagation Using Gaussian Mixture Models and Polynomial Chaos Expansions, Journal of Guidance, Control, and Dynamics, Vol. 39, No. 12, pp. 2615–2626, 2016.

[10] Gerald R. Hintz, Survey of Orbit Element Sets, Journal of Guidance, Control, and Dynamics, Vol. 31, No. 3, pp. 785–790, 2008.

[11] J. T. Kent, I. Hussein, and M. K. Jah, Directional distributions in tracking of space debris, Proceedings of the 19th International Conference on Information Fusion (FUSION), Heidelberg, Germany, IEEE, 2016.

[12] J. T. Kent, The Fisher-Bingham distribution on the sphere, Journal of the Royal Statistical Society, Series B, Vol. 44, 1982, pp. 71-80.

[13] K. V. Mardia, Measures of multivariate skewness and kurtosis with applications. Biometrika- 57 (1970), 519–530.

[14] K. V. Mardia, J. T. Kent, and A. K. Laha, Score matching estimators for directional distributions, ArXiv e-prints, April 2016.

[15] J. T. Kent, S. Bhattacharjee, I. I. Hussein, M. K. Jah,"Bayesian filtering using directional statistics for the orbital tracking problem," Proceedings IAC Australia, Sept 2017 , 2017.

[16] J. H. Jo, I. K. Park, N. Choe, and M. Choi, "The Comparison of the Classical Keplerian Orbit Elements, Non-Singular Orbital Elements (Equinoctial Elements), and the Cartesian State Variables in Lagrange Planetary Equations with J_2 Perturbation: Part I," JASS, 28(1), 37-54 (2011), DOI: 10.5140/JASS.2011.28.1.037.

[17] D. J. Gondelach, R. Armelliny, H. Lewis, J. F. S. Juan, and A. Wittig, "SEMI-ANALYTICAL PROPAGATION WITH DRAG COMPUTATION AND FLOW EXPANSION USING DIFFERENTIAL ALGEBRA," 27th AAS/AIAA Space Flight Mechanics Meeting, San Antonio, United States, 2017.

[18] Richard Fitzpatrick, "Effect of atmospheric drag on artificial satellite orbits", url =https://farside.ph.utexas.edu/teaching/celestial/Celestialhtml, The University of Texas at Austin.

[19] G. E. Cook, "Satellite Drag Coefficients", Planetary and Space Science 13 (1965), 929.

[20] S. Korkmaz, D. Goksuluk, G. Zararsiz, "MVN: An R Package for Assessing Multivariate Normality", The R Journal, 2014, volume = 6, number = 2, 151–162, url =https://journal.r-project.org/archive/2014-2/korkmaz-goksuluk-zararsiz.pdf.